

The effect of set point ratio and surface Young's modulus on maximum tapping forces in fluid tapping mode atomic force microscopy

Bharath Kumar,¹ Phillip M. Pifer,¹ Anthony Giovengo,¹ and Justin Legleiter^{1,2,a)}

¹The C. Eugene Bennett Department of Chemistry, West Virginia University, 217 Clark Hall, P.O. Box 6045, Morgantown, West Virginia 26506, USA

²WVnano Initiative, West Virginia University, 217 Clark Hall, P.O. Box 6045, Morgantown, West Virginia 26506, USA

(Received 14 December 2009; accepted 8 January 2010; published online 22 February 2010; publisher error corrected 2 March 2010)

There is great interest in using proximal probe techniques to simultaneously image and measure physical properties of surfaces with nanoscale spatial resolution. In this regard, there have been recent innovations in generating time-resolved force interaction between the tip and surface during regular operation of tapping mode atomic force microscopy (TMAFM). These tip/sample forces can be used to measure physical material properties of surface in an analogous fashion to the well-established static force curve experiment. Since its inception, it has been recognized that operation of TMAFM in fluids differs significantly from that in air, with one of the major differences manifested in the quality factor (Q) of the cantilever. In air, Q is normally on the order of 200–400, whereas in fluids, it is of the order of approximately 1–5. In this study, we explore the impact of imaging parameters, i.e., set point ratio and free cantilever oscillation amplitude, on time varying tip-sample force interactions in fluid TMAFM via simulation and experiment. The numerical AFM model contains a feedback loop, allowing for the simulation of the entire scanning process. In this way, we explore the impact of varying the Young's modulus of the surface on the maximum tapping force. © 2010 American Institute of Physics. [doi:10.1063/1.3309330]

I. INTRODUCTION

Tapping mode atomic force microscopy (TMAFM) (Ref. 1) is a widely used dynamic imaging technique used to generate three-dimensional topography maps of surfaces with nanoscale spatial resolution by monitoring the amplitude of an oscillating cantilever integrated with an ultrasharp tip probe. In TMAFM, the tip intermittently contacts (or taps) the sample surface, decreasing the cantilever oscillation amplitude from a “free” amplitude A_0 to a tapping amplitude A . The sample surface acts as a repulsive barrier, reducing the tapping amplitude of the cantilever.² With the implementation of a feedback loop to continuously adjust the vertical (z) extension of the piezoelectric scanner to maintain the constant set point ratio $s=A/A_0$, topographical images are obtained by rastering the tip across the surface in the xy plane.

TMAFM can be operated in a fluid environment,^{3–5} which is commonly applied to study biological surfaces under near physiological conditions, to reduce or eliminate capillary forces, and to minimize friction forces. However, it has been recognized that operation of TMAFM in fluids differs significantly in comparison with operation in air,^{4,6–8} with the major difference between operation in air and in fluids being manifested in the quality factor (Q) of the cantilever. While Q is normally on the order of 200–400 for operation in air, Q is reduced to approximately 1–5 for fluid TMAFM, primarily due to the increased hydrodynamic damping in liq-

uids compared to air. The cantilever oscillation when tapping a surface in solution (measured by the deflection signal in the AFM) is characterized by large anharmonicity with a notable sharp distortion which becomes more pronounced with the decrease in set point ratio.

In an effort to more fully understand the interaction between the probe tip and sample surface in TMAFM, cantilever based numerical simulations are often employed.^{6,7,9–19} These simulations have been extensively used to understand the effect of various parameters on tip-sample interactions, such as the time-varying tapping forces, phase, and amplitude. Many of the salient features of fluid TMAFM can be reproduced using a single degree of freedom model characterized by very low Q ($\sim 2-3$).⁷

Due to the physical contact between the probe tip and surface, AFM can be used to ascertain local mechanical properties of the sample. A commonly used method to extract quantitative mechanical information about surfaces exploits AFM's ability to study repulsive and attractive forces between the tip and sample, the so-called “force curve” experiment. In a force curve, the cantilever deflection (which can be converted into force) is recorded as the tip is lowered into contact with the surface, pushed into the sample, and then retracted. Local elasticity and adhesion properties can be quantitatively probed in this manner. Arrays of force curves can be recorded sequentially, and upon extraction of a parameter of interest (slope, pull-out force, etc.), reconstructed into two-dimensional maps, which can be overlaid with topographic images. This method, referred to as force volume imaging, can map local mechanical and elastic properties of surfaces.

^{a)} Author to whom correspondence should be addressed. Electronic mail: justin.legleiter@mail.wvu.edu. Tel.: (304) 293-3435. Ext.: 6436. FAX: (304) 293-4904.

While force curves and force volume imaging have provided valuable insights into the nanoscale mechanical properties of numerous materials,^{20–22} there are several disadvantages to this method. A typical force curve runs at a rate of approximately 1 Hz. At this rate, it would take just over three days to capture a force volume image with 512×512 pixel resolution, a common pixel density of an AFM image. To overcome this issue, the pixel density of a force volume image is often reduced, resulting in an image with much smaller spatial resolution than scanning probe techniques are capable of achieving, creating a situation where spatial resolution is sacrificed for temporal resolution, or vice versa. Furthermore, the maximum force applied to different regions of the surface is nonadaptive. That is, the same force load is applied to softer regions in comparison to harder regions of the surface. This can result in lower resolution caused by larger tip/surface contact area as a result of indentation on softer surfaces, or perhaps more importantly, this can also result in irreversible damage to soft condensed matter or biological surfaces.

Recent AFM technique development efforts have been focused on simultaneously obtaining measurements of physical properties of surfaces while imaging via tapping mode.^{5,23–32} One method to accomplish this goal is the reconstruction of the time-varying force interaction between the tip and surface during regular tapping mode operation. Such tapping force interactions contain information analogous to that accessible via the standard force curve experiment. Of particular interest is the maximum repulsive tapping force, and analytical formulas and scaling laws have been proposed for the maximum repulsive tapping force in both air¹⁹ and solution.³¹

The reconstruction of tapping forces over entire images has been achieved during operation in air^{26–30} and fluid.^{5,31,33} Such an approach offers several experimental advantages over other current AFM techniques. Due to their basis in tapping mode, such methods are nondestructive while maintaining high spatial resolution, both of which are vital in dynamically studying soft, delicate materials. Other methods to quantitatively measure mechanical properties of surfaces (i.e., force volume imaging and nanoindentation) are associated with large deformation depths, resulting in sample damage and decreased resolution. Furthermore, reconstructing tapping forces allows for mapping of surface properties at the same rate of scanning for simple TMAFM imaging, resulting in the ability to dynamically track mechanical changes on surfaces on the timescale of a few minutes. In comparison, force volume image of comparable pixel resolution can take hours to acquire.

In this study, we investigate, via numerical simulation and experiment, the relationship between imaging parameters and the time-varying tapping force on both hard and soft surfaces during TMAFM in solution. We explore the influence of oscillation amplitude and amplitude set point on time-varying tapping forces. We focus on the maximum or peak tapping force per oscillation cycle and how it responds to changes in the Young's modulus of surfaces.

II. EXPERIMENTAL METHODS

A. Numeric simulations of TMAFM

To investigate the relationship between imaging parameters and time-varying tapping forces in solution, numerical simulations were performed with the aid of SIMULINK and MATLAB (MathWorks Inc., Natick, MA). The cantilever was modeled as a single degree of freedom damped driven harmonic oscillator^{2,34–36}

$$m_{\text{eff}}\ddot{z} + b\dot{z} + k[z - D_0 + a_0 \sin(\omega t)] = F_{\text{ext}}, \quad (1)$$

where m_{eff} is the effective mass of a cantilever, b is the damping coefficient, k is the cantilever spring constant, a_0 is the drive amplitude, ω is the drive frequency, D_0 is the resting position of the cantilever base, F_{ext} is the tip-sample force, and z is the position of the cantilever with respect to the surface. While it has been shown that the second mode of the cantilever can play a significant role in cantilever motion near surfaces in fluids,⁶ we make the assumption that such contributions from the second mode are negligible.³¹ In practice, AFM monitors the deflection of the cantilever rather than its position. While the difference between the position and deflection signal is minimal for systems characterized by high values of Q (such as tapping mode operation in air), these signals differ drastically in low Q systems such as observed in fluid tapping AFM.^{4,6–8} Therefore, we monitored the deflection (y) as given by

$$y = z - D_0 + a_0 \sin(\omega t). \quad (2)$$

Thus, Eq. (1) can be re-written in terms of deflection as

$$m_{\text{eff}}[\ddot{y} - a_0\omega^2 \sin(\omega t)] + b[\dot{y} + a_0\omega \cos(\omega t)] + ky = F_{\text{ext}}. \quad (3)$$

In TMAFM, there is a continuously changing separation distance between the probe tip and sample surface due to the oscillation of the cantilever. The probe tip briefly contacts (taps) the surface during each oscillation cycle, resulting in two tip-sample interaction regimes: (1) at large separation distance when the tip and surface are not in contact and (2) when the tip and surface are in contact during the tapping event. The tip near a surface in solution would experience van der Waals forces and electric double layer forces, which is usually described by the Derjaguin–Landau–Verwey–Overbeek (DLVO) theory.³⁷ However, forces arising from the electric double layer effect are negligible due to the high salt concentration used in our experiments, which result in a relatively short Debye length.³¹ Therefore, for large tip-sample separation distance, the external force can be approximated using the van der Waals interaction between a sphere and flat surface³⁷

$$F_{\text{ext}} = -\frac{HR_{\text{tip}}}{6z^2} \quad \text{for } z > a_{\text{DMT}}, \quad (4)$$

where H is the Hamaker constant, R_{tip} is the tip radius, and a_{DMT} is the interatomic distance parameter of a Derjaguin–Muller–Toporov (DMT) potential.³⁸ At the bottom of each oscillation cycle, the probe tip contacts the surface when the separation distance z is smaller than the interatomic distance

(a_{DMT}). Under these conditions, the tip-sample force can be described by a DMT potential.

$$F_{\text{ext}} = \frac{4}{3\pi\kappa_{\text{eff}}}\sqrt{R}(a_{\text{DMT}} - z)^{3/2} - \frac{HR_{\text{tip}}}{6a_{\text{DMT}}^2} \quad \text{for } z \leq a_{\text{DMT}}, \quad (5)$$

with

$$\kappa_{\text{eff}} = \frac{1 - \nu_{\text{tip}}^2}{\pi E_{\text{tip}}} + \frac{1 - \nu_{\text{sample}}^2}{\pi E_{\text{sample}}}, \quad (6)$$

where E_{tip} , ν_{tip} and E_{sample} , ν_{sample} are, respectively, the Young's modulus and Poisson coefficient of the tip and the sample. The effect of altered sample Young's modulus on the imaging process can also be explored by changing the inputs into Eq. (6) and feeding the result into Eq. (5).

The model contained a feedback loop equipped with a proportional-integral-derivative controller (although only the integral gain was used in this study), allowing for the complete simulation of the scanning process in TMAFM over a predetermined surface topography.^{5,13,14} The feedback loop was implemented by measuring the cantilever amplitude, comparing it to the specified set point, and adjusting the cantilever position to maintain the set point using an integral gain. The cantilever amplitude was measured by inspecting the cantilever position signal over the length of one oscillation cycle using signal processing tools available in SIMULINK.

Preparation of bilayer patches. Total brain lipid extract was purchased from Avanti Polar Lipids, dried under a stream of nitrogen, lyophilized, and resuspended in PBS (pH 7.3) at a concentration of 1 mg/ml. By using an acetone/dry-ice bath, bilayers and multilayer lipid sheets were formed by five sequential freeze-thaw cycles.³⁹ The lipid suspensions were then sonicated for 15 min to promote vesicle formation. 40 μl of the suspended vesicle solution, diluted ten times, was added directly to the AFM fluid cell by using the hanging drop method and placed on freshly cleaved mica, allowing vesicles to flatten into small bilayer patches on the surface.

AFM imaging conditions. *In situ* AFM experiments were performed with a Nanoscope V MultiMode scanning probe microscope (Veeco, Santa Barbara, CA) by using a tapping fluid cell equipped with an O-ring and a V-shaped oxide-sharpened silicon nitride cantilever with a nominal spring constant of 0.5 N/m. Images were acquired with a closed-loop "vertical engage" J-scanner. Scan rates were set at 2–3 Hz with cantilever drive frequencies ranging from approximately 8 to 10 kHz, and 5 by 1.25 μm images were captured at 256 \times 64 pixel resolution.

Scanning probe acceleration microscopy (SPAM). SPAM analysis was used to reconstruct every tapping event during AFM imaging as described.⁵ Briefly, cantilever deflection trajectories were simultaneously captured during imaging through an AFM signal access module (Veeco) by using a CompuScope 14-Bit A/D Octopus data acquisition card (Gage Applied Technologies, Lachine, QB, Canada) and custom-written software. Trajectories were captured at 2–5 MS/s and 14-bit resolution with a resolution of 1–2 V. The

trajectory of the cantilever was filtered using a Fourier transform based harmonic comb filter. In this process only intensities corresponding to integer harmonic frequencies are kept, and these are used to reconstruct a deflection signal, $y_{\text{rec}}(t)$, by inverse Fourier transform based on the following equation:

$$y_{\text{rec}}(t) = \mathcal{F}^{-1} \left[y(\omega) \sum_{k=1}^N \delta(\omega - k\omega_{\text{oper}}) \right], \quad (7)$$

where ω_{oper} is the operating frequency and δ is the Dirac's delta function. The summation is carried out up to N , which is the highest harmonic still distinguishable above the noise level. N was typically 20–25 in these experiments. Once $y_{\text{rec}}(t)$ is obtained, the second derivative of the cantilever trajectory is taken and divided by the effective mass, m_{eff} , of the cantilever to obtain the time-resolved based tapping force between the tip and sample based on the following rearrangement of Eq. (3)

$$m_{\text{eff}}\ddot{y} = F_{\text{ext}} + C, \quad (8)$$

with C defined as

$$C = -b\dot{y} - ky + m_{\text{eff}}\omega^2 a_0 \sin(\omega t) - ba_0\omega \cos(\omega t). \quad (9)$$

III. RESULTS AND DISCUSSION

In an effort to understand the effect set point ratio has on the time varying tip-sample force associated with TMAFM in solution, single degree of freedom simulations were performed with parameters based on the typical properties of commercially available silicon nitride cantilevers. These parameters were: drive frequency of 8–10 kHz, spring constant of 0.5 N/m, and free amplitude of 40 nm. The simulation parameters were chosen to correspond to imaging a 1 μm line with a scan rate of 1 Hz. As TMAFM is commonly used to image a variety of surfaces, we performed simulations of TMAFM on a simulated surface containing a 5 nm step with a Young's moduli of 60 GPa surrounding the step and 2.5 GPa on the step. These simulations employed a feedback loop to actively maintain the set point ratio while scanning the cantilever across the model surface. Simulations were performed at a series of set point ratios while keeping all other parameters constant. The shape of simulated cantilever deflection trajectories very well reproduced the characteristic shape commonly observed in real fluid TMAFM experiments, containing large anharmonic distortions that increased with the lower set point ratios [Fig. 1(a)]. As the tapping amplitude approaches the cantilever free amplitude, the distortion appeared nearer the trough of the trajectory and was less pronounced. The distortion associated with the tapping interaction on the 2.5 GPa portion of the surface was subtly less pronounced in comparison to that occurring on the 60 GPa areas.

Individual time varying tip-sample force interactions obtained from numerical simulations are shown for the 60 and 2.5 GPa portions of the model surfaces in Fig. 1(b). The maximum force (F_{max}) and total tip/sample force (F_{tot}) per oscillation cycle were investigated. F_{max} is defined as the peak or largest force experienced between the tip and

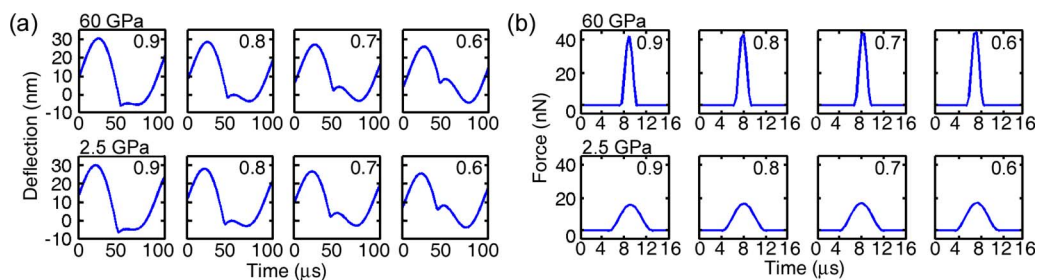


FIG. 1. (Color online) Results of numerical simulations of fluid TMAFM on a model surface containing a soft step (2.5 GPa) on a more rigid surface (60 GPa). (a) Simulated deflection signals of TMAFM on the 60 and 2.5 GPa portions of the model surface reproduced the characteristic shape commonly observed in real fluid TMAFM experiments, i.e., large anharmonic distortions that increased as a function of set point ratio. (b) Simulated tapping force pulses between the tip and the 60 or 2.5 GPa are shown as a function of set point ratio. As the set point ratio was decreased, the maximum tapping force (F_{\max}) increased. For any given set point ratio, F_{\max} was always larger on the 60 GPa surface compared to the 2.5 GPa surface.

sample. F_{tot} is defined as the sum of the entire tip/sample force interaction over one cantilever oscillation cycle or the force integrated over one cycle. On both surfaces, the tapping force (both maximum and total force per oscillation) systematically increased as the set point ratio was changed from 0.9 to 0.6. While the F_{tot} between the tip and surface per oscillation cycle remained constant for any given set point ratio (total force on 60 GPa surface was the same as on the 2.5 GPa surface), closer inspection of these simulated force profiles revealed that for any given set point ratio that F_{\max} was higher on the 60 GPa surface in comparison to the softer 2.5 GPa surface with a corresponding longer contact time for the softer surface, suggesting that F_{\max} may provide a convenient measure of local Young's modulus. The dependence of F_{\max} on surface modulus indicates the potential use of F_{\max} as a measurement of modulus while imaging; however, the ability to use F_{\max} for such measurements is dependent on how F_{\max} changes with operating conditions.

Due to the observed changes in F_{\max} with surface modulus, we further explored the relative changes in F_{\max} as set point ratio was changed for different surfaces (Fig. 2). The

rationale for this exploration was to determine if relative F_{\max} values on different surfaces are independent of the set point ratio, which would allow for the use of F_{\max} to measure values of Young's modulus of surfaces without complications associated with imaging conditions. We first systematically changed the separation distance between the simulated oscillating cantilever and the model surfaces (60 and 2.5 GPa) while monitoring the tapping forces and actual tapping amplitude, which was used to calculate the set point ratio [Fig. 2(a)]. The change observed F_{\max} on both surfaces are similar to those observed in previous work which proposed scaling laws for peak tapping forces.³¹ This systematic change for both surfaces as a function of set point ratio suggested that values of F_{\max} on different surfaces may change predictably relative to each other. We next determined the relative relationships between F_{\max} on the respective model surfaces as a function of set point ratio. The relationships explored as a function of set point ratio were (1) the ratio of F_{\max} on the soft surface to the F_{\max} on the hard surface [Fig. 2(b)] and (2) the difference between the F_{\max} on the respective surfaces [Fig. 2(c)]. The ratio of F_{\max} on different sur-

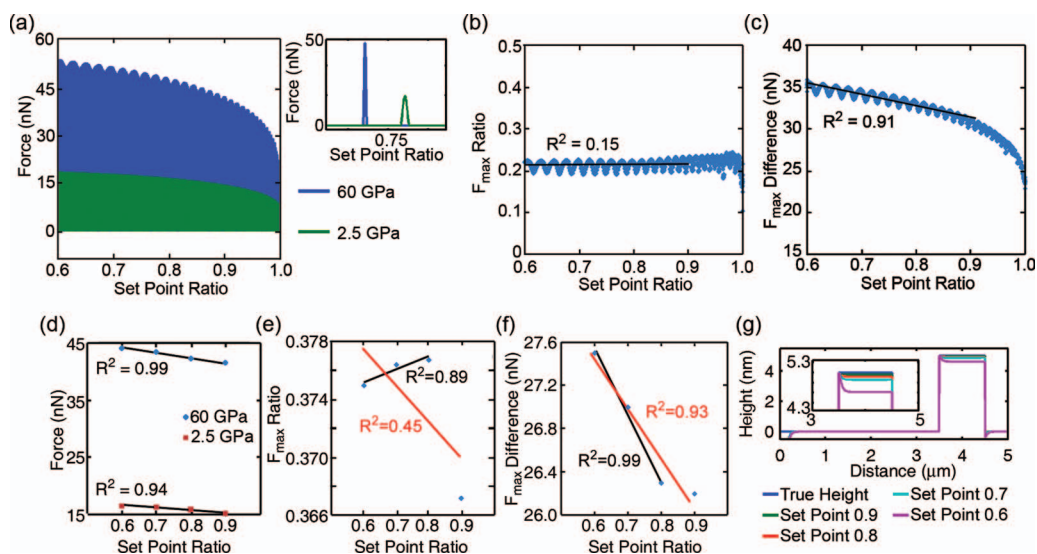


FIG. 2. (Color) Numerically simulate tip/sample interaction forces on a hard (60 GPa) and soft (2.5 GPa) surfaces as a function of set point ratio. [(a), (b), (c), and (d)] F_{\max} increased systematically as a function of decreasing set point ratio on both surfaces. The relationships between the relative F_{\max} on the two surfaces was explored as a function of set point ratio by examining, (e) the ratio of F_{\max} on the soft surface to the F_{\max} on the hard surface, and (f) the difference between the F_{\max} on the respective surfaces. (g) A series of simulated scan lines taken over the soft model step are shown as a function of set point ratio (inset zooms in on the top of the step). As the set point ratio is decreased, compression of the soft step systematically increased.

faces has been suggested as a potential way to calibrate tapping forces to extract relative values of the surface moduli by direct comparison with the ratio of the respective values of Young's moduli.⁵ We were concerned primarily with the range of set point ratio from 0.6 to 0.9, as this is a commonly used range of set points for actual tapping mode imaging. In the 0.9–0.6 range of set point ratios, there did not appear to be a simple relationship with the ratios of F_{\max} on the respective surfaces; however, this may have been due to the large oscillations observed in the tapping forces associated with the 60 GPa surface. Despite these oscillations, the F_{\max} difference between the two surfaces as a function of set point ratio in the range of 0.6–0.9 was quite linear ($R^2=0.91$).

Next, we explored the relative changes in F_{\max} associated with 60 and 2.5 GPa surface as a function of set point ratio controlled via the feedback loop, which is more similar to the actual AFM imaging process. We performed these simulations at four different set point ratios (0.9, 0.8, 0.7, and 0.6). One advantage of this type of simulation was that oscillating force interactions were not observed on the 60 GPa model surface. On both the 60 and 2.5 GPa surface, F_{\max} decreased linearly with increased set point ratio [Fig. 2(d)]. As a function of set point ratio, the F_{\max} ratio [Fig. 2(e)] in simulation again did not change in a linear manner ($R^2=0.45$); however, removing the ratio measured at set point ratio of 0.9, at which the probe is barely tapping the surface, dramatically improved linearity ($R^2=0.89$). When looking at the difference between the F_{\max} [Fig. 2(f)] on the different model surfaces, a much more linear relationship was observed even with the inclusion of set point ratio of 0.9 ($R^2=0.93$). With the removal of the F_{\max} difference measured at set point ratio 0.9, the linearity improves ($R^2=0.99$). This suggests that, while tapping forces increase with a decreased set point ratio, the relative difference in F_{\max} on surfaces of differing Young's modulus changes predictably in the narrow range commonly used for TMAFM imaging in solution.

While maximum tapping force increased with smaller set point ratios in simulation, we next determined the impact of these increased forces on the process of acquiring an image of the model surface containing a 5 nm tall step. The AFM model was able to track the surface step under all simulation conditions; however, the height of the trace over the step was consistently smaller than the actual step height. This reduced measured step height was caused by the different compressibility, or softness, of the step in comparison to its more rigid surroundings. This phenomenon is the basis of compliance-based contrast commonly observed in TMAFM. The compression of the soft step increased as the set point ratio was lowered, due to the higher tapping forces associated with lower set point ratios.

To verify experimentally the relationship between set point ratio and tip-sample maximum tapping forces in solution, we imaged supported bilayer patches (soft surface with Young's modulus of approximately 1–3 GPa) on mica (hard surface with a Young's modulus of approximately 60 GPa) using fluid TMAFM. We performed experiments at three different free amplitudes (20, 40, and 60 nm) and set point ratios (0.9, 0.8, 0.7, and 0.6). Results for the 60 nm free amplitude experiments are shown in Fig. 3. While the height

images [Fig. 3(a)] of the supported bilayers were obtained, the entire cantilever deflection trajectory was captured, digitized, comb-filtered using a sliding window Fourier transform as described earlier, used to reconstruct the tip/sample force interaction of every individual tapping event, and each individual tap was used to reconstruct an F_{\max} image of the surface [Fig. 3(b)]. Individual filtered cantilever deflection trajectories for tapping regions corresponding to mica or bilayer are shown for different set point ratios in Fig. 3(c). Similar to simulation, the distortion in the sinusoidal cantilever motion due to the physical contact with the surface appeared nearer the trough of the trajectory and was less pronounced as the tapping amplitude approaches the cantilever free amplitude. While the tap occurs at the same portion of the oscillation cycle for any given set point ratio, the distortion associated with the tapping interaction on a bilayer is subtly less pronounced in comparison to that occurring on mica.

Time resolved tip/sample tapping forces corresponding to mica or bilayer are shown for different set point ratios in Fig. 3(d). Since the effective modulus of the bilayer on mica is much lower than the modulus of bare mica, the tapping force pulses on mica were taller (greater F_{\max}) and narrower than force pulses on the bilayer for any given set point ratio [Fig. 3(d)]. On both surfaces, the F_{\max} systematically increased as the set point ratio was changed from 0.9 to 0.6 [Fig. 3(d)] similar to simulation but the F_{\max} associated with tapping the bilayer surface was always smaller in comparison with taps on mica. Histograms of maximum tapping force over the entire reconstructed force image [Fig. 3(e)] were distinctly bimodal with modes corresponding to the mica and bilayer surfaces at all set point ratios and free amplitudes. However, the separation between the distributions of measured F_{\max} on bilayer and mica is often less pronounced at a set point ratio of 0.9, at which the probe is just striking the surface. This feature was also observed in simulation that used the feedback loop to maintain the set point ratio. Similar results were observed at free cantilever amplitudes of 20 and 40 nm respectively (Supplemental Figs. 1 and 2).⁴⁰ The average F_{\max} on mica or bilayer for different free amplitudes decreased linearly (R^2 ranging from 0.86–0.99) as set point ratio increased (Fig. 4).

Next, we explored the relative changes in F_{\max} associated with the mica and bilayer surface as a function of set point ratio (Fig. 5). The ratio of F_{\max} associated with the bilayer to F_{\max} on mica was not strongly linear (R^2 values ranging from 0.55 to 0.99) as a function of set point for most experiments, even when removing data from set point ratios of 0.9 as suggested by simulation. The ratio was always larger when operating at larger free amplitudes for any given cantilever, suggesting that this ratio is highly dependent on imaging conditions and potentially difficult to interpret as a method for extracting mechanical information of surfaces. The difference between F_{\max} on the two surfaces did not appear to be highly linear with the inclusion of data when the set point ratio was 0.9 (R^2 values ranging from 0.72–0.96); however, the linearity (R^2 at least 0.9 for all conditions) dramatically improved with the exclusion of data from when the set point ratio was 0.9 (just tapping). Unlike the F_{\max} ratio,

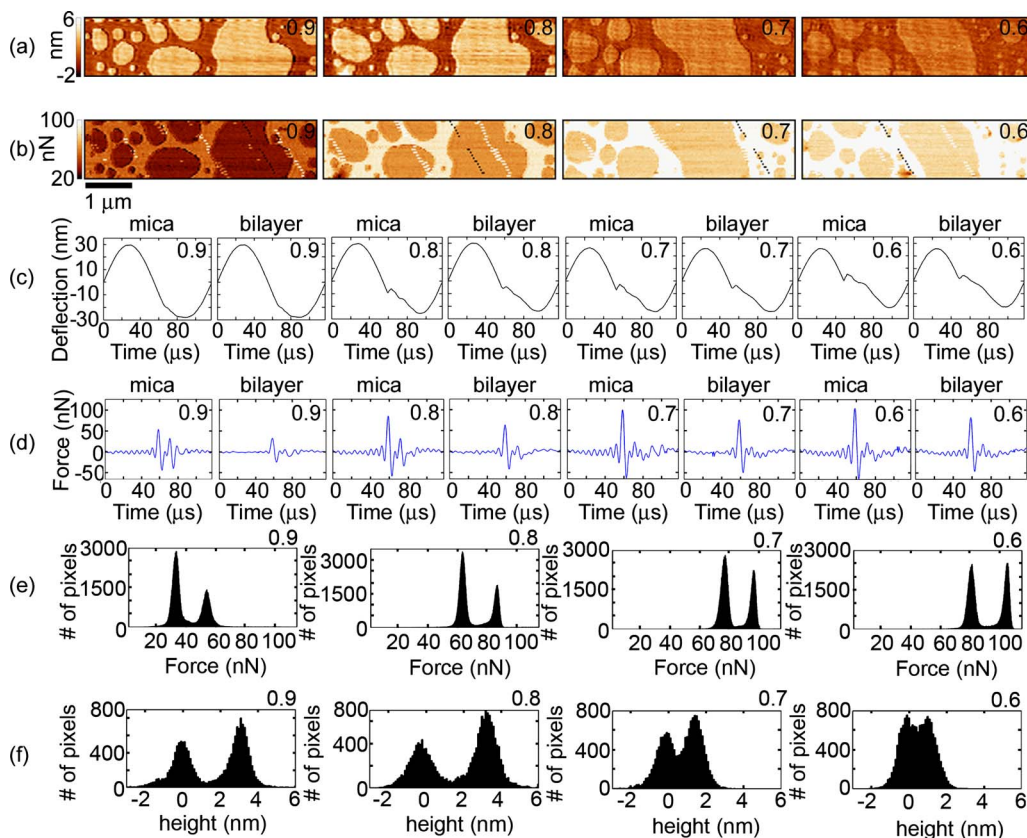


FIG. 3. (Color online) A series of fluid TMAFM images of supported brain lipid extract bilayer patches on mica during the entire cantilever deflection trajectory was captured and used to reconstruct the tip/sample force interaction of every individual tapping event for experiments with free cantilever oscillation amplitude of 60 nm. All images were captured with the same cantilever during one experiment. (a) TMAFM height images of bilayer patches at various set point ratios as indicated in the upper left hand corner of each image. The height color bar is applicable to each height image. (b) Reconstructed F_{\max} images of the supported lipid bilayer patches on mica at different set point ratios corresponding to the height image directly above it. The F_{\max} color bar is applicable to each reconstructed force image. (c) Individual captured cantilever deflection trajectories at each set point ratio (as indicated) corresponding to tapping events on mica or bilayer. (d) Reconstructed individual force pulses corresponding to tapping events on mica or bilayer for the indicated set point ratios. (e) F_{\max} of every individual tap from the reconstructed F_{\max} images and the (f) height of each individual pixel from the height images of supported bilayer patches on mica at the indicated set point ratios.

the F_{\max} difference did not appear correlated with free oscillation amplitude. Similar to simulation, these characteristics suggest that the relative difference in F_{\max} on surfaces of differing Young's modulus changes predictably, and could thus be used to estimate the Young's modulus of surfaces while imaging as long as the tapping amplitude does not approach the free amplitude.

As the tip-sample forces associated with imaging resulted in reduced height measurement of the soft step in simulation due to compliance of the sample with a dependence on set point ratio, we next determined if this was also the case for our experimental system. For tapping in air, it has been shown that compression of soft polystyrene features increases linearly with F_{\max} under a variety of imaging conditions,¹³ and it has been demonstrated that tapping forces play a role in the ability to reliably image soft viral capsids in solution.³¹ For the mica/bilayer system explored here, the observed height and the ability to adequately image the bilayer appeared to be more dependent on the actual set point ratio rather than F_{\max} . Histograms of the measured height of each pixel in the AFM images revealed that the observed height of the bilayer changes with set point ratio [Fig. 3(e)]. At larger set point ratios (0.9 and 0.8) the

measured height ($\sim 3\text{--}4$ nm) approached the theoretical height of the bilayer (~ 5 nm); whereas, the observed height of the bilayer patches decreased to 1–2 nm when operating at a set point ratios of 0.7 or 0.6. Despite larger maximum tapping forces with increased free amplitude, the average height measurements were similar for the same set point ratio at values of free amplitude (Fig. 6). Taken collectively, these observations indicated that height measurements of supported bilayers imaged in this study were highly dependent on the portion of the oscillation cycle during which the tip

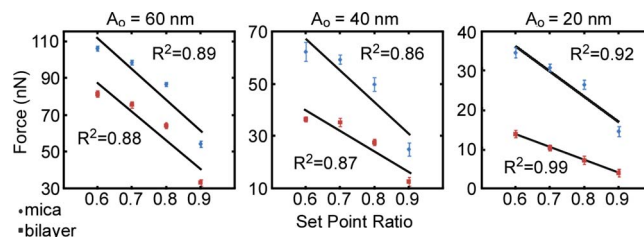


FIG. 4. (Color online) Average F_{\max} values measured on mica (blue) or bilayer (red) surfaces during TMAFM experiments in solution as a function of set point ratio. The free oscillation amplitude of the cantilever (A_0) was 60, 40, or 20 nm respectively.

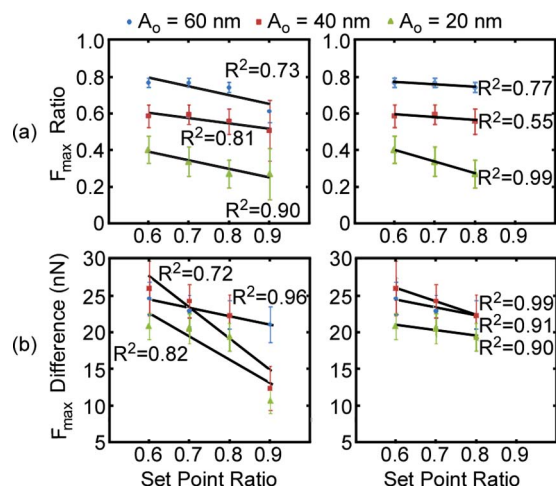


FIG. 5. (Color online) The relative changes in F_{\max} associated with the mica and bilayer surface are explored as a function of set point ratio by calculating (a) the ratio of F_{\max} on the bilayer:mica surface and (b) the F_{\max} difference between the mica and bilayer surface. All four set point values were used to calculate R^2 values on the left plots; whereas, data for set point ratio 0.9 was excluded on the right plots.

contacts the surface, which is altered with changes in set point ratio.

IV. CONCLUSIONS

One of the major thrusts in the field of scanning probe techniques is to combine imaging capabilities with simultaneous measurements of physical properties. In TMAFM, the most straightforward way to accomplish this is to reconstruct the time-resolved force interaction between the tip and surface. However, the force interaction between the tip and surface in TMAFM has been shown to be highly dependent on operating conditions. Such knowledge of tip-sample forces can be used for mapping material properties with nanoscale spatial resolution. In this regard, great strides have been made to accomplish reconstruction of time-resolved tapping forces. In order to glean quantitative information from such experiments, it is imperative to understand how exogenous experimental conditions influence the observed tip/surface interactions. Presented results and simulations demonstrate that the maximum observed tapping force for TMAFM op-

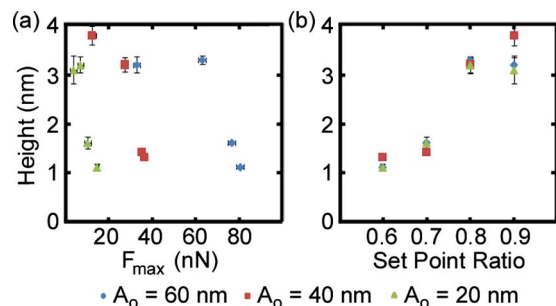


FIG. 6. (Color online) Measured average heights of supported bilayers on mica are shown as a function of (a) F_{\max} and (b) set point ratio for free cantilever oscillation amplitudes of 60 (blue), 40 (red), and 20 nm (green).

eration in fluids is directly related to material stiffness and operating conditions such as cantilever oscillation free amplitude and the amplitude set point. Based on analytical formulas, it has been suggested that these two parameters have the most influence on peak repulsive or maximum tapping forces.¹⁹ Results presented here demonstrate that the relative changes in F_{\max} on surfaces can be used to estimate the respective local Young's modulus while imaging in TMAFM in solution without concern about changes associated with free amplitude or set point ratio.

ACKNOWLEDGMENTS

This work was supported by West Virginia University (start-up package, JL). PMP was supported by the Summer Undergraduate Research Experience program (West Virginia University).

- ¹Q. Zhong, D. Inniss, K. Kjoller, and V. B. Elings, *Surf. Sci.* **290**, L688 (1993).
- ²N. A. Burnham, O. P. Behrend, F. Oulevey, G. Gremaud, P.-J. Gallo, D. Gourdon, E. Dupas, A. J. Kulik, H. M. Pollock, and G. A. D. Briggs, *Nanotechnology* **8**, 67 (1997).
- ³P. K. Hansma, J. P. Cleveland, M. Radmacher, D. A. Walters, P. E. Hillner, M. Bezanilla, M. Fritz, D. Vie, H. G. Hansma, C. B. Prater, J. Massie, L. Fukunaga, J. Gurley, and V. Elings, *Appl. Phys. Lett.* **64**, 1738 (1994).
- ⁴C. A. J. Putman, K. O. Van der Werf, B. G. De Grooth, N. F. Van Hulst, and J. Greve, *Appl. Phys. Lett.* **64**, 2454 (1994).
- ⁵J. Legleiter, M. Park, B. Cusick, and T. Kowalewski, *Proc. Natl. Acad. Sci. U.S.A.* **103**, 4813 (2006).
- ⁶S. Basak and A. Raman, *Appl. Phys. Lett.* **91**, 064107 (2007).
- ⁷J. Legleiter and T. Kowalewski, *Appl. Phys. Lett.* **87**, 163120 (2005).
- ⁸M. J. Martin, H. K. Fathy, and B. H. Houston, *J. Appl. Phys.* **104**, 044316 (2008).
- ⁹R. Garcia and R. Perez, *Surf. Sci. Rep.* **47**, 197 (2002).
- ¹⁰A. S. Paulo and R. Garcia, *Phys. Rev. B* **66**, 041406 (2002).
- ¹¹T. R. Rodriguez and R. Garcia, *Appl. Phys. Lett.* **80**, 1646 (2002).
- ¹²N. Hashemi, H. Dankowicz, and M. R. Paul, *J. Appl. Phys.* **103**, 094511 (2008).
- ¹³J. Legleiter, *Nanotechnology* **20**, 245703 (2009).
- ¹⁴T. Kowalewski and J. Legleiter, *J. Appl. Phys.* **99**, 064903 (2006).
- ¹⁵L. Zitzler, S. Herminghaus, and F. Mugele, *Phys. Rev. B* **66**, 155436 (2002).
- ¹⁶A. Varol, I. Gunev, B. Orun, and C. Basdogan, *Nanotechnology* **19**, 075503 (2008).
- ¹⁷A. Raman, J. Melcher, and R. Tung, *Nanotoday* **3**, 20 (2008).
- ¹⁸J. Melcher, S. Hu, and A. Raman, *Appl. Phys. Lett.* **91**, 053101 (2007).
- ¹⁹S. Hu and A. Raman, *Appl. Phys. Lett.* **91**, 123106 (2007).
- ²⁰X. Xin, M. Hussain, and J. J. Mao, *Cell. Molec. Biol. Tech. Biomater. Eval.* **28**, 316 (2007).
- ²¹J. Solon, I. Levental, K. Sengupta, P. C. Georges, and P. A. Janmey, *Biophys. J.* **93**, 4453 (2007).
- ²²A. E. Pelling, D. W. Dawson, D. M. Carreon, J. J. Christiansen, R. R. Shen, M. A. Teitell, and J. K. Gimzewski, *Nanomedicine* **3**, 43 (2007).
- ²³M. Stark, R. W. Stark, W. M. Heckl, and R. Guckenberger, *Proc. Natl. Acad. Sci. U.S.A.* **99**, 8473 (2002).
- ²⁴R. W. Stark and W. M. Heckl, *Rev. Sci. Instrum.* **74**, 5111 (2003).
- ²⁵R. Hillenbrand, M. Stark, and R. Guckenberger, *Appl. Phys. Lett.* **76**, 3478 (2000).
- ²⁶O. Sahin, *Rev. Sci. Instrum.* **78**, 103707 (2007).
- ²⁷O. Sahin, *Isr. J. Chem.* **48**, 55 (2008).
- ²⁸O. Sahin, *Phys. Rev. B* **77**, 115405 (2008).
- ²⁹O. Sahin and N. Erina, *Nanotechnology* **19**, 445717 (2008).
- ³⁰O. Sahin, S. Magonov, C. Su, C. F. Quate, and O. Solgaard, *Nat. Nanotechnol.* **2**, 507 (2007).
- ³¹X. Xu, C. Carrasco, P. J. de Pablo, J. Gomez-Herrero, and A. Raman, *Biophys. J.* **95**, 2520 (2008).
- ³²X. Xu, J. Melcher, S. Basak, R. Reifengerger, and A. Raman, *Phys. Rev. B* **102**, 060801 (2009).
- ³³M. Dong, S. Husale, and O. Sahin, *Nat. Nanotechnol.* **4**, 514 (2009).

- ³⁴A. Kühle, A. H. Sorensen, and J. Bohr, *J. Appl. Phys.* **81**, 6562 (1997).
- ³⁵M. V. Salapaka, D. J. Chen, and J. P. Cleveland, *Phys. Rev. B* **61**, 1106 (2000).
- ³⁶Y. X. Song and B. Bhushan, *J. Phys.: Condens. Matter* **20**, 225011 (2008).
- ³⁷J. Israelachvili, *Intermolecular & Surface Forces* (Academic, London, 1992).
- ³⁸B. V. Derjaguin, V. M. Muller, and Y. P. Toporov, *J. Colloid Interface Sci.* **53**, 314 (1975).
- ³⁹C. M. Yip, E. A. Elton, A. A. Darabie, M. R. Morrison, and J. McLaurin, *J. Mol. Biol.* **311**, 723 (2001).
- ⁴⁰See supplementary material at <http://dx.doi.org/10.1063/1.3309330> for a series of fluid tapping mode AFM images of supported brain lipid extract bilayer patches on mica during the entire cantilever deflection trajectory captured and used to reconstruct the tip/sample force interaction of every individual tapping event for experiments with free cantilever oscillation amplitude of 40 and 20 nm.